






Quantum Inverse Contextual Vision Transformers (Q-ICVT): A New Frontier in 3D Object Detection for AVs

Sanjay Bhargav Dharavath 
 Indian Institute of Technology
 Kharagpur, India
 sanjaytinku810@gmail.com

Tanmoy Dam 
 Emory University,
 USA
 tanmoydam@yahoo.com

Supriyo Chakraborty 
 Indian Institute of Technology
 Kharagpur, India
 supriyochakraborty@iitkgp.ac.in

Prithwiraj Roy 
 Global Action Alliance
 Washington, USA
 przhr@mst.edu

Aniruddha Maiti 
 ADP
 New Jersey, USA
 aniruddha.maiti87@gmail.com

ABSTRACT

The field of autonomous vehicles (AVs) predominantly leverages multi-modal integration of LiDAR and camera data to achieve better performance compared to using a single modality. However, the fusion process encounters challenges in detecting distant objects due to the disparity between the high resolution of cameras and the sparse data from LiDAR. Insufficient integration of global perspectives with local-level details results in sub-optimal fusion performance. To address this issue, we have developed an innovative two-stage fusion process called Quantum Inverse Contextual Vision Transformers (Q-ICVT). This approach leverages adiabatic computing in quantum concepts to create a novel reversible vision transformer known as the Global Adiabatic Transformer (GAT). GAT aggregates sparse LiDAR features with semantic features in dense images for cross-modal integration in a global form. Additionally, the Sparse Expert of Local Fusion (SELF) module maps the sparse LiDAR 3D proposals and encodes position information of the raw point cloud onto the dense camera feature space using a gating point fusion approach. Our experiments show that Q-ICVT achieves an mAPH of 82.54 for L2 difficulties on the Waymo dataset, improving by 1.88% over current state-of-the-art fusion methods. We also analyze GAT and SELF in ablation studies to highlight the impact of Q-ICVT. Our code is available at [Q-ICVT](#).



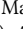

CCS CONCEPTS

• **Computing methodologies** → **Computer vision problems**.

KEYWORDS

GAT; SELF; Multi-Modal Fusion; 3D Object Detection

ACM Reference Format:

Sanjay Bhargav Dharavath , Tanmoy Dam , Supriyo Chakraborty , Prithwiraj Roy , and Aniruddha Maiti . 2024. Quantum Inverse Contextual Vision Transformers (Q-ICVT): A New Frontier in 3D Object Detection

Permission to make digital or hard copies of all or part of this work for personal or classroom use is granted without fee provided that copies are not made or distributed for profit or commercial advantage and that copies bear this notice and the full citation on the first page. Copyrights for components of this work owned by others than the author(s) must be honored. Abstracting with credit is permitted. To copy otherwise, or republish, to post on servers or to redistribute to lists, requires prior specific permission and/or a fee. Request permissions from permissions@acm.org.

CIKM '24, October 21–25, 2024, Boise, ID, USA

© 2024 Copyright held by the owner/author(s). Publication rights licensed to ACM.

ACM ISBN 979-8-4007-0436-9/24/10

<https://doi.org/10.1145/3627673.3679984>

for AVs. In *Proceedings of the 33rd ACM International Conference on Information and Knowledge Management (CIKM '24)*, October 21–25, 2024, Boise, ID, USA. ACM, New York, NY, USA, 6 pages. <https://doi.org/10.1145/3627673.3679984>

1 RELATED WORK

LiDAR based 3D OD: LiDAR point clouds, which are typically unordered collections of data points, can be divided into three main types: voxel-based, point-based, and point-voxel fusion methods. Voxel-based techniques, as indicated in studies like [3, 8, 16], convert point cloud data into voxels and then use deep sparse convolution layers to extract features. Point-based methods, referenced in [3, 40], involve using stacked Multi-Layer Perceptrons (MLPs) to process raw point cloud data and obtain point-level features. Unlike earlier studies, recent works [10, 45] have introduced hybrid methods that combine point and voxel-based representations for more comprehensive feature extraction.

Multi-modal Integration for 3D OD: Integrating monocular vision with LiDAR point clouds enhances 3D object detection [2, 18, 41, 43, 44]. Monocular systems infer 3D bounding boxes from 2D images but lack depth information [43], addressed by estimating pixel-level depth [43]. Recognizing objects in 2D images often precedes analyzing point cloud data [27, 32, 47], typically using a two-step, object-centered fusion approach [17, 32]. Mid-level fusion strategies, like local-global fusion methods [7, 21] and other approaches [31, 56], combine 2D and 3D data by transferring information across their respective backbones. However, optimal alignment between camera and LiDAR features remains a major challenge [21]. Additionally, maintaining matching camera characteristics becomes complex when numerous LiDAR points are combined within a single 3D voxel [7]. To address this challenge, we have introduced a novel two-stage fusion method, known as Q-ICVT. Our main contributions are defined as follows:

- We introduce an adiabatic computing-inspired transformer, GAT, to align sparse voxelized features with dense image features in a global context.
- We develop the sparse attention of gating experts, SELF, to achieve local fusion between RoI features and dense image features.

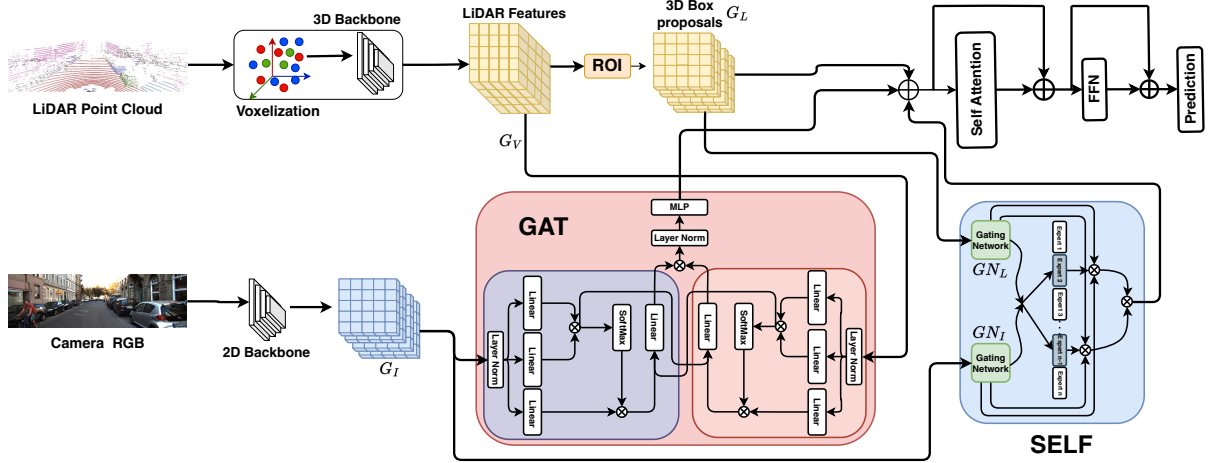


Figure 1: Q-ICVT Pipeline: We have introduced two novel fusion blocks from extracted sparse LiDAR features (G_V) and dense image data (G_I). GAT is designed based on the adiabatic computing concept to match between the two modalities by global pointwise attention. Similarly, in SELF, the voxelized local RoI proposal feature (G_L) is combined with a gating mechanism with G_I at the local-level fusion.

2 METHODOLOGY

LiDAR and Image Feature Estimation Let's define the multi-modal input-output sequences as $\{(I_j, L_j), (I_{(j-1)}, L_{(j-1)}), \dots\}$ for simplicity. Each input sequence at the j -th step consists of two types of data: LiDAR, referred to as L_j , and a camera image, represented by $x \in I_j \in \mathbb{R}^{H \times W \times 3}$. The raw LiDAR point cloud for the j -th input is denoted as $L_j \rightarrow Q_j^{raw}$, with $Q_j^{raw} = (\mathcal{U}_p, \mathcal{V}_p, \mathcal{W}_p, \mathcal{G}_p)_{p=1}^N$, where N represents the total number of points. Our objective is to design a robust local-global fusion integration to obtain adequate performance. The input point cloud data from the j -th position (Q) is converted into a voxelized representation with the coordinates $U \times V \times W \times C_V$; this representation is represented by the symbol G_V . The calculation of voxel features involves the mean value of point-wise features applied to non-empty voxels [7, 21]. The farthest point sampling (FPS) technique is employed for determining critical points [38]. This results in the generation of \mathcal{K} crucial points ($G_V^{\mathcal{K}}$), where \mathcal{K} is defined as 4096 for WOD. Then, the average of attributes from each point within the voxel is computed to characterize non-empty voxels, such as three-dimensional coordinates and reflectance values. Following this, a sequence of $3 \times 3 \times 3$ 3D sparse convolutions [39] are performed on the feature volumes of the point cloud. This results in the downsampling of spatial resolutions by $1\times$, $2\times$, $4\times$, and $8\times$, respectively. Following that, hierarchical intra-voxel regions (RoI) are obtained using a region proposal network [7, 21, 39] to generate initial bounding box proposals. Consequently, the sparse LiDAR feature is represented as $G_V \in \mathbb{R}^{H_V \times W_V \times C_V}$. Similarly, dense semantic image features $G_I \in \mathbb{R}^{H_I \times W_I \times C_I}$ are obtained using a 2D detector [25, 35].

2.1 Adiabatic computing in GAT

In the context of vision transformers [13, 55], the main goal is to utilize the reversibility of adiabatic processes [4, 20, 33, 34] to improve the global context and effectively handle the interaction between

two modalities: LiDAR point cloud ($G_V \in \mathbb{R}^{H_V \times W_V \times C_V}$) and image data ($G_I \in \mathbb{R}^{H_I \times W_I \times C_I}$). In order to assess the reversibility process, both forward and backward transformations were conducted between two distinct feature modalities. One modality was represented in a sparse form using LiDAR, while the other modality was represented in a dense form retrieved from the input image.

Let us consider a reversible block in a transformer layer, as illustrated in Figure 1. The GAT module is capable of effectively handling sparse and dense modalities through forward and reverse mechanisms [12]. To attain this objective, we first consider the forward transition through linear projection data as a global query [13] with key-value pair matching. These forward mechanism transformer blocks help retain not only the focus on the central forward points around the voxelized sparse feature (G_V), but also identify affine matrices within the dense image (G_I). Unlike existing methods [21, 28], the global spatial resolution around the voxelized LiDAR point feature (G_V) does not guarantee a comprehensive sense of the dense image feature (G_I). Therefore, we also introduce another reversible transformer block for query-key-value matching of the voxelized LiDAR feature [29], which will be considered as the backward transition of the matrix. Therefore, the forward transformation block in GAT is defined as follows:

$$Y_f = \mathcal{F}(G_I) \quad (1)$$

where $\mathcal{F} \in \mathbb{R}^{H_I \times W_I \times C_I}$ is the forward transformer block [14]. Here, $Q, K, V \in G_I$ and we use layer normalization in between the query-key-value matching [13]. Similarly, the backward transformation for the voxelized LiDAR feature is represented as follows:

$$Y_r = \mathcal{F}^{-1}(G_V) \quad (2)$$

where $\mathcal{F}^{-1} \in \mathbb{R}^{H_V \times W_V \times C_V}$ is the backward transformer block [14]. Here, $Q, K, V \in G_V$, and we use layer normalization similar to the forward path [29]. To accumulate the dimension matching, we

concatenate the matrix transition through a linear layer. Therefore, we concatenate the forward and reverse blocks in GAT using the \oplus operation. Finally, the GAT model is obtained as follows:

$$G_{VI} = \mathcal{G}(Y_f \oplus Y_r) \quad (3)$$

where \oplus denotes the concatenation operation. $G_{VI} \in \mathbb{R}^{H_I \times W_I \times C_I}$ ensures that the original dense image feature (G_I) can be retrieved.

2.2 Sparse Expert of Local Fusion (SELF)

To achieve local-level fusion, we introduce Sparse Expert fusion for voxelized LiDAR data. A region proposal network [7, 21, 39] generates initial bounding box suggestions ($P = \{P_1, P_2, \dots, P_n\}$) based on multi-level voxel features (G_V). The multi-level voxel features of RoI are defined by G_L . We adopt the Mixture of Experts (MoE) [36, 37] model, known for capturing long dependencies in heterogeneous sequence datasets [6, 11, 50], for sparse RoI LiDAR features (G_L) and dense image features (G_I). This robust framework leverages specialized sub-models or "experts," each optimized for different input subsets. We extend two separate gating networks (A gating network determines the weights for each expert), $GN_L(\cdot)$ for LiDAR and $GN_I(\cdot)$ for image data, to determine the weights for each gating networks. For a given LiDAR input G_L and an image input G_I , the outputs of both modalities are computed as:

$$y_L = \sum_{i=1}^N GN_{Li}(G_L)E_{Li}(G_L) \quad (4)$$

$$y_I = \sum_{i=1}^N GN_{Ii}(G_I)E_{Ii}(G_I) \quad (5)$$

where, y_L and y_I are each gating mechanism outputs for each modalities passing through by selecting by expert networks. N numbers of experts for each modalities. Therefore, the gating network(GN) is defined as follows,

$$GN(x) = \text{Softmax}(\text{TopK}(\mathbb{H}_w(x), k)) \quad (6)$$

where, $\mathbb{H}_w(x)$ is the individual gating function that can be represented by the parametric weight w , $\mathbb{H}_w(x) = \Psi(\text{Softplus}(x \cdot \delta))$, where δ is the noise [24].

$E(\cdot)$ is an expert network function that will choose top K values. Therefore, selecting TopK experts from $E(\cdot)$ is represented as follows [5],

$$\{E_{L/I,k}\}_{k=1}^N = \begin{cases} E_{L/I,j} & \text{if } j \in \arg \max_{1:K} \{GN_{L/I,j}\}_{j=1}^N \\ -\infty & \text{otherwise} \end{cases} \quad (7)$$

These dual-gating mechanism (Equ. 7 and Equ. 6) allows the model to independently assess and integrate the specific characteristics of each modality. By doing so, the model can more effectively capture the complementary information provided by LiDAR and image data. The final fused output y is then derived by combining y_L and y_I through a subsequent fusion network \mathbb{F} :

$$y = \mathbb{F}(y_L, y_I) \quad (8)$$

where \mathbb{F} can be easily obtained through an embedding function. This method fuses distinct data types to boost multimodal task performance.

3 EXPERIMENTAL VALIDATION

3.1 Dataset Details

WOD achieves excellent performance in 3D object detection benchmarks, thanks to its extensive dataset consisting of more than 200,000 frames, 1,150 sequences, and a combination of LiDAR, images [42]. The dataset comprises 798 training sequences, 202 validation sequences, and 150 testing sequences. The detection range is 75 meters, and the coverage area is 150 meters by 150 meters. We evaluate models using Average Precision (AP) and Average Precision weighted by Heading (APH) as described in [21, 42]. We include results for both LEVEL_1 (L1) and LEVEL_2 (L2) difficulty items, offering a thorough assessment and comparison of the models' performance.

3.2 Evolution of WOD performance

The detailed performance of Q-ICVT, both single and ensemble variants, on the WOD test and validation sets is presented in Table 1 and Table 2. According to Table 1, Q-ICVT excels, surpassing other leading methods in both L1 and L2 difficulty levels. Compared to LoGoNet [21], Q-ICVT shows significant gains, especially in L2 difficulty with a 1.24 increase in APH value, achieved without ensemble techniques. Specifically, the non-ensemble version of Q-ICVT outperforms LoGoNet [21] by 1.22 AP/L1, 1.14 APH/L1, 1.15 AP/L2, and 0.80 APH/L2 for vehicles; 1.12 AP/L1, 1.38 APH/L1, 1.34 AP/L2, and 1.56 APH/L2 for pedestrians; and 1.80 AP/L1, 1.08 APH/L1, 0.98 AP/L2, and 1.35 APH/L2 for cyclists, leading to a total improvement of 1.24 mAPH/L2. The ensemble version of Q-ICVT also surpasses LoGoNet-Ens [21] with differences of 0.88 AP/L1, 1.11 APH/L1, 1.29 AP/L2, and 0.97 APH/L2 for vehicles; 0.03 AP/L1, 0.47 APH/L1, 1.65 AP/L2, and 2.54 APH/L2 for pedestrians; and 1.61 AP/L1, 1.85 APH/L1, 1.48 AP/L2, and 1.06 APH/L2 for cyclists, resulting in an overall improvement of 1.52 mAPH/L2.

Table 2 presents an extensive comparison of model performance for 3D object detection on the WOD validation set. Remarkably, Q-ICVT shows substantial advancements across various difficulty levels. For L1 difficulty, it surpasses the validation results of LoGoNet [21] on WOD by 2.91 AP/L1, 2.24 APH/L1, 5.48 AP/L2, and 3.99 APH/L2 for vehicles; 2.70 AP/L1, 2.80 APH/L1, 3.71 AP/L2, and 2.36 APH/L2 for pedestrians; and 2.96 AP/L1, 2.77 APH/L1, 2.27 AP/L2, and 1.66 APH/L2 for cyclists, resulting in an overall improvement of 2.67 mAPH/L2. These improvements highlight Q-ICVT proficiency in accurately detecting all classes, emphasizing the effectiveness of multi-modal feature alignment in enhancing 3D object detection.

4 ABLATION STUDIES ON WOD

Influence of each component. Table 3 highlights the effects of individual components on L2 difficulty in the QICVT WOD test set. When only the Global Adiabatic Transformer (GAT) is used without the Sparse Expert of Local Fusion (SELF), performance decreases to 79.56 for vehicles, 80.12 for pedestrians, and 78.97 for cyclists. This drop is due to the limitations of the SELF component, which fails to

Table 1: Evaluation of Model Performance for 3D Detection on the WOD Test Set. In this table, ‘L’ represents LiDAR sensors, ‘T’ represents camera sensors, ‘TTA’ stands for test-time augmentation, and ‘Ens’ denotes ensemble model outputs, marked by #.

Method	Modality	ALL (mAPH)	VEH (AP/APH)		PED (AP/APH)		CYC (AP/APH)	
		L2	L1	L2	L1	L2	L1	L2
Q-ICVT Ens (ours) #	L+I	82.54 (+1.52)	89.21/88.98	83.46/82.69	89.01/86.43	85.92/83.82	84.71/84.01	82.41/81.12
LoGoNet Ens# [21]	L+I	81.02	88.33/87.87	82.17/81.72	88.98/85.96	84.27/81.28	83.10/82.16	80.93/80.06
BEVFusion TTA# [26]	L+I	79.97	87.96/87.58	81.29/80.92	87.64/85.04	82.19/79.65	82.53/81.67	80.17/79.33
LidarMultiNet TTA# [53]	L	79.94	87.64/87.26	80.73/80.36	87.75/85.07	82.48/79.86	82.77/81.84	80.50/79.59
MPPNet Ens# [3]	L	79.60	87.77/87.37	81.33/80.93	87.92/85.15	82.86/80.14	80.74/79.90	78.54/77.73
MT-Net Ens# [1]	L	78.45	87.11/86.69	80.52/80.11	86.50/83.55	80.95/78.08	80.50/79.43	78.22/77.17
DeepFusion Ens# [22]	L+I	78.41	86.45/86.09	79.43/79.09	86.14/83.77	80.88/78.57	80.53/79.80	78.29/77.58
AFDetV2 Ens# [16]	L	77.64	85.80/85.41	78.71/78.34	85.22/82.16	79.71/76.75	81.20/80.30	78.70/77.83
INT Ens# [48]	L	77.21	85.63/85.23	79.12/78.73	84.97/81.87	79.35/76.36	79.76/78.65	77.62/76.54
HoriLiDAR3D Ens# [9]	L+I	77.11	85.09/84.68	78.23/77.83	85.03/82.10	79.32/76.50	79.73/78.78	77.91/76.98
Q-ICVT (ours)	L+I	78.34 (+1.24)	87.73/87.24	80.84/80.10	87.96/85.53	82.89/80.47	77.86/76.33	74.87/74.45
LoGoNet [21]	L+I	77.10	86.51/86.10	79.69/79.30	86.84/84.15	81.55/78.91	76.06/75.25	73.89/73.10
BEVFusion [26]	L+I	76.33	84.97/84.55	77.88/77.48	84.72/81.97	79.06/76.41	78.49/77.54	76.00/75.09
CenterFormer [57]	L	76.29	85.36/84.94	78.68/78.28	85.22/82.48	80.09/77.42	76.21/75.32	74.04/73.17
MPPNet [3]	L	75.67	84.27/83.88	77.29/76.91	84.12/81.52	78.44/75.93	77.11/76.36	74.91/74.18
DeepFusion [22]	L+I	75.54	83.25/82.82	76.11/75.69	84.63/81.80	79.16/76.40	77.81/76.82	75.47/74.51

Table 2: Comparative Performance Analysis on the Waymo Validation Set for 3D Vehicle Detection (IoU = 0.7), Pedestrian Detection (IoU = 0.5), and Cyclist Detection (IoU = 0.5). PV-RCNN [38] is our baseline model.

Method	Modality	ALL (mAPH)	VEH (AP/APH)		PED (AP/APH)		CYC (AP/APH)	
		L2	L1	L2	L1	L2	L1	L2
SECOND [49]	L	57.23	72.27/71.69	63.85/63.33	68.70/58.18	60.72/51.31	60.62/59.28	58.34/57.05
PointPillars [19]	L	57.53	71.60/71.00	63.10/62.50	70.60/56.70	62.90/50.20	64.40/62.30	61.90/59.90
LiDAR-RCNN [23]	L	60.10	73.50/73.00	64.70/64.20	71.20/58.70	63.10/51.70	68.60/66.90	66.10/64.40
CenterPoint[54]	L	65.46	-	-/66.20	-	-/62.60	-	-/67.60
PointAugmenting [46]	L+I	66.70	67.4/-	62.7/-	75.04/-	70.6/-	76.29/-	74.41/-
Pyramid-PV [30]	L	-	76.30/75.68	67.23/66.68	-	-	-	-
PDV [15]	L	64.25	76.85/76.33	69.30/68.81	74.19/65.96	65.85/58.28	68.71/67.55	66.49/65.36
Graph-RCNN [51]	L	70.91	80.77/80.28	72.55/72.10	82.35/76.64	74.44/69.02	75.28/74.21	72.52/71.49
3D-MAN [52]	L	-	74.50/74.00	67.60/67.10	71.70/67.70	62.60/59.00	-	-
Centerformer [57]	L	73.70	78.80/78.30	74.30/73.80	82.10/79.30	77.80/75.00	75.20/74.40	73.20/72.30
DeepFusion [22]	L+I	-	80.60/80.10	72.90/72.40	85.80/83.00	78.70/76.00	-	-
MPPNet [3]	L	74.22	81.54/81.06	74.07/73.61	84.56/81.94	77.20/74.67	77.15/76.50	75.01/74.38
MPPNet [3]	L	74.85	82.74/82.28	75.41/74.96	84.69/82.25	77.43/75.06	77.28/76.66	75.13/74.52
LoGoNet [21]	L+I	75.54	83.21/82.72	75.84/75.38	85.80/83.14	78.97/76.33	78.58/77.79	75.67/74.91
Baseline[38]	L	63.33	77.51/76.89	68.98/68.41	75.01/65.65	66.04/57.61	67.81/66.35	65.39/63.98
Q-ICVT (ours)	L+I	78.21 (+14.88)	86.12/84.96	81.32/79.37	88.50/85.94	82.68/78.69	81.54/80.56	77.94/76.57

achieve optimal fusion despite integrating voxel RoI features into the GAT module. The exclusion of GAT leads to an even greater decline in performance: 78.27 for vehicles, 79.51 for pedestrians, and 77.34 for cyclists. Therefore, even though local fusion centroids are closer to the image surface, voxel point centroids are not able to provide dense image feature information, diminishing the effectiveness of global cross-modal fusion. Combining both GAT and SELF components results in significant performance improvements, with scores of 82.69 for vehicles, 83.82 for pedestrians, and 81.12 for cyclists, underscoring the importance of both components for optimal performance.

5 CONCLUSION

We introduced QICVT, a 3D multi-modal object detection method based on transformers, consisting of two key components: GAT and SELF. These components were designed to capture both local and global dependencies, thereby enhancing the efficacy of 3D

Table 3: Each component’s effect on L2 difficulty in the Q-ICVT WOD test set

Components		APH (L2)		
GAT	SELF	VEH	PED	CYC
✓		79.56	80.12	78.97
	✓	78.27	79.51	77.34
✓	✓	82.69	83.82	81.12

detection at both short and long distances. To determine the efficacy of QICVT, we conducted comprehensive experiments on the WOD benchmark datasets. QICVT demonstrated its efficacy in multi-modal object detection by achieving competitive performance when compared to state-of-the-art methods. In addition, we conducted comprehensive ablation experiments to compare the effect of each proposed component on QICVT’s performance.

REFERENCES

- [1] Shaoxiang Chen, Zequn Jie, Xiaolin Wei, and Lin Ma. 2022. MT-Net Submission to the Waymo 3D Detection Leaderboard. *arXiv preprint arXiv:2207.04781* (2022).
- [2] Xiaozhi Chen, Kaustav Kundu, Ziyu Zhang, Huimin Ma, Sanja Fidler, and Raquel Urtasun. 2016. Monocular 3d object detection for autonomous driving. In *Proceedings of the IEEE conference on computer vision and pattern recognition*. 2147–2156.
- [3] Xuesong Chen, Shaoshuai Shi, Benjin Zhu, Ka Chun Cheung, Hang Xu, and Hongsheng Li. 2022. Mppnet: Multi-frame feature intertwining with proxy points for 3d temporal object detection. In *European Conference on Computer Vision*. Springer, 680–697.
- [4] Carlo Ciliberto, Mark Herbster, Alessandro Davide Ialongo, Massimiliano Pontil, Andrea Rocchetto, Simone Severini, and Leonard Wossnig. 2018. Quantum machine learning: a classical perspective. *Proceedings of the Royal Society A: Mathematical, Physical and Engineering Sciences* 474, 2209 (2018), 20170551.
- [5] Tanmoy Dam. 2022. *Developing generative adversarial networks for classification and clustering: Overcoming class imbalance and catastrophic forgetting*. Ph.D. Dissertation. UNSW Sydney.
- [6] Tanmoy Dam, Sreenatha G Anavatti, and Hussein A Abbass. 2021. Improving clusterGAN using self-augmented information maximization of disentangling latent spaces. *arXiv preprint arXiv:2107.12706* (2021).
- [7] Tanmoy Dam, Sanjay Bhargav Dharavath, Sameer Alam, Nimrod Yildiz, Supriyo Chakraborty, and Mir Feroshkan. 2024. AYDIV: Adaptable Yielding 3D Object Detection via Integrated Contextual Vision Transformer. *arXiv preprint arXiv:2402.07680* (2024).
- [8] Jiajun Deng, Shaoshuai Shi, Peiwei Li, Wengang Zhou, Yanyong Zhang, and Houqiang Li. 2021. Voxel R-CNN: Towards High Performance Voxel-based 3D Object Detection. *arXiv:2012.15712 [cs.CV]*
- [9] Zhuangzhuang Ding, Yihan Hu, Runzhou Ge, Li Huang, Sijia Chen, Yu Wang, and Jie Liao. 2020. 1st Place Solution for Waymo Open Dataset Challenge–3D Detection and Domain Adaptation. *arXiv preprint arXiv:2006.15505* (2020).
- [10] Lue Fan, Ziqi Pang, Tianyuan Zhang, Yu-Xiong Wang, Hang Zhao, Feng Wang, Naiyan Wang, and Zhaoxiang Zhang. 2022. Embracing single stride 3d object detector with sparse transformer. In *Proceedings of the IEEE/CVF Conference on Computer Vision and Pattern Recognition*. 8458–8468.
- [11] Xing Han, Huy Nguyen, Carl Harris, Nhat Ho, and Suchi Saria. 2024. FuseMoE: Mixture-of-Experts Transformers for Fleximodal Fusion. *arXiv preprint arXiv:2402.03226* (2024).
- [12] Stuart M Harwood, Dimitar Trenev, Spencer T Stober, Panagiotis Barkoutsos, Tanvi P Gujarati, Sarah Mostame, and Donny Greenberg. 2022. Improving the variational quantum eigensolver using variational adiabatic quantum computing. *ACM Transactions on Quantum Computing* 3, 1 (2022), 1–20.
- [13] Ali Hatamizadeh, Hongxu Yin, Greg Heinrich, Jan Kautz, and Pavlo Molchanov. 2023. Global context vision transformers. In *International Conference on Machine Learning*. PMLR, 12633–12646.
- [14] Ali Hatamizadeh, Hongxu Yin, Jan Kautz, and Pavlo Molchanov. 2022. Global context vision transformers. *arXiv preprint arXiv:2206.09959* (2022).
- [15] Jordan SK Hu, Tianshu Kuai, and Steven L Waslander. 2022. Point density-aware voxels for lidar 3d object detection. In *Proceedings of the IEEE/CVF Conference on Computer Vision and Pattern Recognition*. 8469–8478.
- [16] Yihan Hu, Zhuangzhuang Ding, Runzhou Ge, Wenxin Shao, Li Huang, Kun Li, and Qiang Liu. 2022. Afdetv2: Rethinking the necessity of the second stage for object detection from point clouds. In *Proceedings of the AAAI Conference on Artificial Intelligence*, Vol. 36, 969–979.
- [17] Jason Ku, Melissa Mozifian, Jungwook Lee, Ali Harakeh, and Steven L Waslander. 2018. Joint 3d proposal generation and object detection from view aggregation. In *2018 IEEE/RSJ International Conference on Intelligent Robots and Systems (IROS)*. IEEE, 1–8.
- [18] Jason Ku, Alex D Pon, and Steven L Waslander. 2019. Monocular 3d object detection leveraging accurate proposals and shape reconstruction. In *Proceedings of the IEEE/CVF conference on computer vision and pattern recognition*. 11867–11876.
- [19] Alex H Lang, Sourabh Vora, Holger Caesar, Lubing Zhou, Jiong Yang, and Oscar Beijbom. 2019. Pointpillars: Fast encoders for object detection from point clouds. In *Proceedings of the IEEE/CVF conference on computer vision and pattern recognition*. 12697–12705.
- [20] Ming Li and Paul Vitányi. 1996. Reversibility and adiabatic computation: trading time and space for energy. *Proceedings of the Royal Society of London. Series A: Mathematical, Physical and Engineering Sciences* 452, 1947 (1996), 769–789.
- [21] Xin Li, Tao Ma, Yuenan Hou, Botian Shi, Yuchen Yang, Youquan Liu, Xingjiao Wu, Qin Chen, Yikang Li, Yu Qiao, et al. 2023. LoGoNet: Towards Accurate 3D Object Detection with Local-to-Global Cross-Modal Fusion. In *Proceedings of the IEEE/CVF Conference on Computer Vision and Pattern Recognition*. 17524–17534.
- [22] Yingwei Li, Adams Wei Yu, Tianjian Meng, Ben Caine, Jiquan Ngiam, Daiyi Peng, Junyang Shen, Bo Wu, Yifeng Lu, Denny Zhou, Quoc V. Le, Alan Yuille, and Mingxing Tan. 2022. DeepFusion: Lidar-Camera Deep Fusion for Multi-Modal 3D Object Detection. *arXiv:2203.08195 [cs.CV]*
- [23] Zhichao Li, Feng Wang, and Naiyan Wang. 2021. Lidar r-cnn: An efficient and universal 3d object detector. In *Proceedings of the IEEE/CVF Conference on Computer Vision and Pattern Recognition*. 7546–7555.
- [24] Bin Lin, Zhenyu Tang, Yang Ye, Jiayi Cui, Bin Zhu, Peng Jin, Junwu Zhang, Munan Ning, and Li Yuan. 2024. Moe-llava: Mixture of experts for large vision-language models. *arXiv preprint arXiv:2401.15947* (2024).
- [25] Ze Liu, Yutong Lin, Yue Cao, Han Hu, Yixuan Wei, Zheng Zhang, Stephen Lin, and Baining Guo. 2021. Swin transformer: Hierarchical vision transformer using shifted windows. In *Proceedings of the IEEE/CVF international conference on computer vision*. 10012–10022.
- [26] Zhijian Liu, Haotian Tang, Alexander Amini, Xinyu Yang, Huizi Mao, Daniela L Rus, and Song Han. 2023. BevFusion: Multi-task multi-sensor fusion with unified bird’s-eye view representation. In *2023 IEEE International Conference on Robotics and Automation (ICRA)*. IEEE, 2774–2781.
- [27] Zhijian Liu, Xinyu Yang, Haotian Tang, Shang Yang, and Song Han. 2023. FlatFormer: Flattened Window Attention for Efficient Point Cloud Transformer. In *Proceedings of the IEEE/CVF Conference on Computer Vision and Pattern Recognition*. 1200–1211.
- [28] Tao Ma, Xuemeng Yang, Hongbin Zhou, Xin Li, Botian Shi, Junjie Liu, Yuchen Yang, Zhizheng Liu, Liang He, Yu Qiao, et al. 2023. Detzero: Rethinking offboard 3d object detection with long-term sequential point clouds. In *Proceedings of the IEEE/CVF International Conference on Computer Vision*. 6736–6747.
- [29] Karttikeya Mangalam, Haoqi Fan, Yanghao Li, Chao-Yuan Wu, Bo Xiong, Christoph Feichtenhofer, and Jitendra Malik. 2022. Reversible vision transformers. In *Proceedings of the IEEE/CVF Conference on Computer Vision and Pattern Recognition*. 10830–10840.
- [30] Jiageng Mao, Minzhe Niu, Haoyue Bai, Xiaodan Liang, Hang Xu, and Chunjing Xu. 2021. Pyramid r-cnn: Towards better performance and adaptability for 3d object detection. In *Proceedings of the IEEE/CVF International Conference on Computer Vision*. 2723–2732.
- [31] AJ Piergiovanni, Vincent Casser, Michael S Ryoo, and Anelia Angelova. 2021. 4d-net for learned multi-modal alignment. In *Proceedings of the IEEE/CVF International Conference on Computer Vision*. 15435–15445.
- [32] Charles R Qi, Wei Liu, Chenxia Wu, Hao Su, and Leonidas J Guibas. 2018. Frustum pointnets for 3d object detection from rgb-d data. In *Proceedings of the IEEE conference on computer vision and pattern recognition*. 918–927.
- [33] Varadi Rajesh, Umesh Parameshwar Naik, et al. 2021. Quantum Convolutional Neural Networks (QCNN) using deep learning for computer vision applications. In *2021 International conference on recent trends in electronics, information, communication & technology (RTEICT)*. IEEE, 728–734.
- [34] Andreas Rauchenecker, Timm Ostermann, and Robert Wille. 2017. Exploiting reversible logic design for implementing adiabatic circuits. In *2017 MIXDES-24th International Conference "Mixed Design of Integrated Circuits and Systems"*. IEEE, 264–270.
- [35] Shaoqing Ren, Kaiming He, Ross Girshick, and Jian Sun. 2015. Faster r-cnn: Towards real-time object detection with region proposal networks. *Advances in neural information processing systems* 28 (2015).
- [36] Carlos Riquelme, Joan Puigcerver, Basil Mustafa, Maxim Neumann, Rodolphe Jenatton, André Susano Pinto, Daniel Keysers, and Neil Houlsby. 2021. Scaling vision with sparse mixture of experts. *Advances in Neural Information Processing Systems* 34 (2021), 8583–8595.
- [37] Noam Shazeer, Azalia Mirhoseini, Krzysztof Maziarz, Andy Davis, Quoc Le, Geoffrey Hinton, and Jeff Dean. 2017. Outrageously large neural networks: The sparsely-gated mixture-of-experts layer. *arXiv preprint arXiv:1701.06538* (2017).
- [38] Shaoshuai Shi, Chaoxu Guo, Li Jiang, Zhe Wang, Jianping Shi, Xiaogang Wang, and Hongsheng Li. 2020. Pv-rccnn: Point-voxel feature set abstraction for 3d object detection. In *Proceedings of the IEEE/CVF Conference on Computer Vision and Pattern Recognition*. 10529–10538.
- [39] Shaoshuai Shi, Xiaogang Wang, and Hongsheng Li. 2019. Pointcnn: 3d object proposal generation and detection from point cloud. In *Proceedings of the IEEE/CVF conference on computer vision and pattern recognition*. 770–779.
- [40] Weijing Shi and Raj Rajkumar. 2020. Point-gnn: Graph neural network for 3d object detection in a point cloud. In *Proceedings of the IEEE/CVF conference on computer vision and pattern recognition*. 1711–1719.
- [41] Xuepeng Shi, Zhixiang Chen, and Tae-Kyun Kim. 2023. Multivariate Probabilistic Monocular 3D Object Detection. In *Proceedings of the IEEE/CVF Winter Conference on Applications of Computer Vision*. 4281–4290.
- [42] Pei Sun, Henrik Kretschmar, Xerxes Dotiwalla, Aurelien Chouard, Vijaysai Patnaik, Paul Tsui, James Guo, Yin Zhou, Yuning Chai, Benjamin Caine, Vijay Vasudevan, Wei Han, Jiquan Ngiam, Hang Zhao, Aleksei Timofeev, Scott Ettinger, Maxim Krivokon, Amy Gao, Aditya Joshi, Sheng Zhao, Shuyang Cheng, Yu Zhang, Jonathon Shlens, Zhifeng Chen, and Dragomir Anguelov. 2020. Scalability in Perception for Autonomous Driving: Waymo Open Dataset. *arXiv:1912.04838 [cs.CV]*
- [43] Chongben Tao, JieCheng Cao, Chen Wang, Zufeng Zhang, and Zhen Gao. 2023. Pseudo-Mono for Monocular 3D Object Detection in Autonomous Driving. *IEEE Transactions on Circuits and Systems for Video Technology* (2023).

- [44] Runzhou Tao, Wencheng Han, Zhongying Qiu, Cheng-zhong Xu, and Jianbing Shen. 2023. Weakly Supervised Monocular 3D Object Detection using Multi-View Projection and Direction Consistency. In *Proceedings of the IEEE/CVF Conference on Computer Vision and Pattern Recognition*. 17482–17492.
- [45] Sourabh Vora, Alex H Lang, Bassam Helou, and Oscar Beijbom. 2020. Pointpainting: Sequential fusion for 3d object detection. In *Proceedings of the IEEE/CVF conference on computer vision and pattern recognition*. 4604–4612.
- [46] Chunwei Wang, Chao Ma, Ming Zhu, and Xiaokang Yang. 2021. Pointaugmenting: Cross-modal augmentation for 3d object detection. In *Proceedings of the IEEE/CVF Conference on Computer Vision and Pattern Recognition*. 11794–11803.
- [47] Zhixin Wang and Kui Jia. 2019. Frustum convnet: Sliding frustums to aggregate local point-wise features for amodal 3d object detection. In *2019 IEEE/RSJ International Conference on Intelligent Robots and Systems (IROS)*. IEEE, 1742–1749.
- [48] Jianyun Xu, Zhenwei Miao, Da Zhang, Hongyu Pan, Kaixuan Liu, Peihan Hao, Jun Zhu, Zhengyang Sun, Hongmin Li, and Xin Zhan. 2022. Int: Towards infinite-frames 3d detection with an efficient framework. In *European Conference on Computer Vision*. Springer, 193–209.
- [49] Yan Yan, Yuxing Mao, and Bo Li. 2018. Second: Sparsely embedded convolutional detection. *Sensors* 18, 10 (2018), 3337.
- [50] Deshun Yang, Luhui Hu, Yu Tian, Zihao Li, Chris Kelly, Bang Yang, Cindy Yang, and Yuexian Zou. 2024. WorldGPT: a Sora-inspired video AI agent as Rich world models from text and image inputs. *arXiv preprint arXiv:2403.07944* (2024).
- [51] Honghui Yang, Zili Liu, Xiaopei Wu, Wenxiao Wang, Wei Qian, Xiaofei He, and Deng Cai. 2022. Graph r-cnn: Towards accurate 3d object detection with semantic-decorated local graph. In *European Conference on Computer Vision*. Springer, 662–679.
- [52] Zetong Yang, Yin Zhou, Zhifeng Chen, and Jiquan Ngiam. 2021. 3d-man: 3d multi-frame attention network for object detection. In *Proceedings of the IEEE/CVF Conference on Computer Vision and Pattern Recognition*. 1863–1872.
- [53] Dongqiangzi Ye, Zixiang Zhou, Weijia Chen, Yufei Xie, Yu Wang, Panqu Wang, and Hassan Foroosh. 2023. Lidarmultinet: Towards a unified multi-task network for lidar perception. In *Proceedings of the AAAI Conference on Artificial Intelligence*, Vol. 37. 3231–3240.
- [54] Tianwei Yin, Xingyi Zhou, and Philipp Krahenbuhl. 2021. Center-based 3d object detection and tracking. In *Proceedings of the IEEE/CVF conference on computer vision and pattern recognition*. 11784–11793.
- [55] Pengchuan Zhang, Xiyang Dai, Jianwei Yang, Bin Xiao, Lu Yuan, Lei Zhang, and Jianfeng Gao. 2021. Multi-scale vision longformer: A new vision transformer for high-resolution image encoding. In *Proceedings of the IEEE/CVF international conference on computer vision*. 2998–3008.
- [56] Chaoda Zheng, Xu Yan, Haiming Zhang, Baoyuan Wang, Shenghui Cheng, Shuguang Cui, and Zhen Li. 2022. Beyond 3d siamese tracking: A motion-centric paradigm for 3d single object tracking in point clouds. In *Proceedings of the IEEE/CVF Conference on Computer Vision and Pattern Recognition*. 8111–8120.
- [57] Zixiang Zhou, Xiangchen Zhao, Yu Wang, Panqu Wang, and Hassan Foroosh. 2022. Centerformer: Center-based transformer for 3d object detection. In *European Conference on Computer Vision*. Springer, 496–513.